

Constraint Satisfaction Programming for the No-three-in-line Problem

Thomas Prellberg

*School of Mathematical Sciences
Queen Mary University of London
United Kingdom*

Abstract

Using a constraint satisfaction approach, we exhibit configurations of $2n$ points on the $n \times n$ grid for all $n \leq 60$ with no three collinear. Consequently, the smallest n for which it is unknown whether $D(n) = 2n$ increases from 47 to 61.

Keywords: No-three-in-line problem, Lattice points, Combinatorial geometry, Constraint programming

2020 MSC: 05B40, 52C10

1. Introduction

The no-three-in-line problem, first posed more than one hundred years ago for a chessboard by Henry Dudeney [3, Puzzle 317], asks for the maximum number $D(n)$ of lattice points that can be selected from the $n \times n$ points of the square lattice so that no three lie on a common line [8, 13]. An obvious upper bound is $D(n) \leq 2n$, and for large n it is conjectured that $D(n) < cn$ with $c = \pi/\sqrt{3} \approx 1.81$ using a probabilistic estimate[7]. Best known constructions for large n give configurations with $\frac{3}{2}n - o(n)$ lattice points based on modular hyperbolas [9]. Recent extensions include generalizations to the infinite square grid [14] and to higher dimensions [12]. It is worth noting that the classical no-three-in-line problem discussed here is a special case of the general position problem in combinatorial geometry and graphs, as surveyed in [1].

Until recently, examples with $D(n) = 2n$ were known only for $n \leq 46$ and for $n = 48, 50, 52$ [5, 6]. Harborth, Oertel, and Prellberg [10] showed that symmetry reduction is an effective way to reduce the search space; this was also key in [5, 6], where known solutions for large n had 90° rotational symmetry for n even, or 90° rotational symmetry except for the diagonal for n odd (augmented by two symmetric points on one diagonal). The work presented here also makes use of these symmetries.

There has been renewed interest in the computational aspect of this and related problems, applying modern techniques such as integer programming, reinforcement learning, and AI [4, 2, 16]. Using a computer search based on constraint satisfaction and CP-SAT

Email address: `t.prellberg@qmul.ac.uk` (Thomas Prellberg)

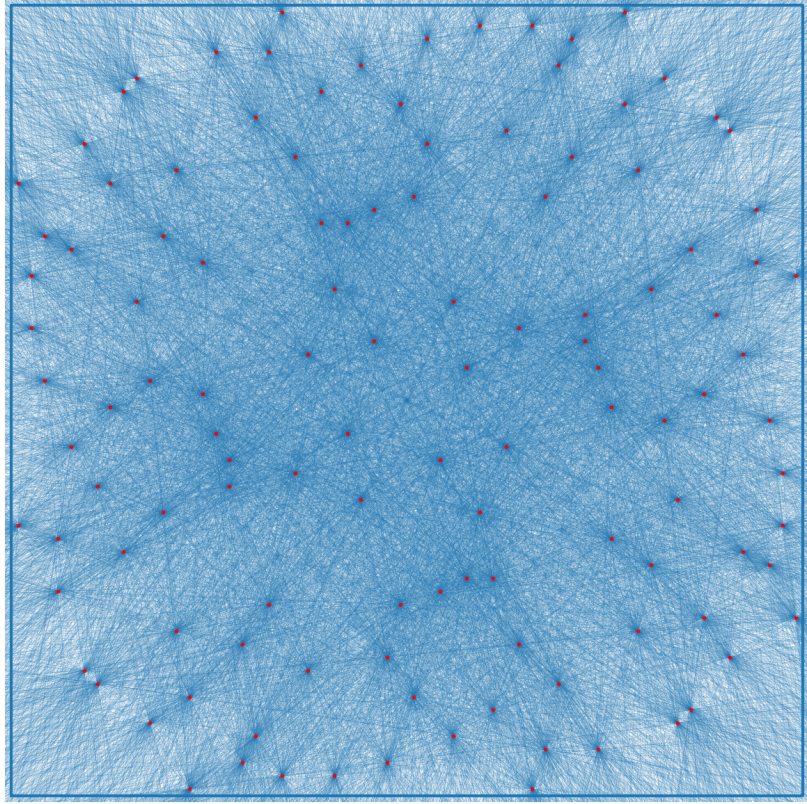


Figure 1: $2n$ lattice points with no three in line for $n = 60$. The 120 occupied sites (red) are shown together with the $\binom{120}{2} = 7140$ straight-line segments joining each pair of occupied sites (blue), illustrating the 90° rotational symmetry.

[15], we find configurations with $D(n) = 2n$ for all $n \leq 60$. Figure 1 shows the largest such configuration at $n = 60$. Thus the smallest n for which it is unknown whether $D(n) = 2n$ is 61.

We conclude this section with detailing the probabilistic counting heuristic from [7]. Let G_n be the square grid of n^2 points, and let t_n denote the number of collinear triples in G_n ,

$$t_n = 2 \sum_{a=1}^{n-1} \sum_{b=1}^{n-1} (n-a)(n-b) \gcd(a, b) - \frac{1}{6} n^2 (n^2 - 1) = \frac{3}{\pi^2} n^4 \log n + O(n^4).$$

A uniformly random triple of points is collinear with probability $q_n = t_n/\binom{n^2}{3}$. Now choose a k -subset $T \subset G_n$ uniformly at random. There are $\binom{k}{3}$ triples inside T . Approximating the events that these triples are collinear as independent (a crude but convenient heuristic), we estimate

$$\mathbb{P}(T \text{ contains no collinear triple}) \approx (1 - q_n)^{\binom{k}{3}}.$$

Multiplying by the number of candidate sets gives the heuristic count

$$C(n, k) = \binom{n^2}{k} (1 - q_n)^{\binom{k}{3}}.$$

Next fix $\lambda > 0$ and set $k = \lfloor \lambda n \rfloor$. Using standard asymptotics for $\binom{n^2}{k}$ with $k = O(n)$ and the expansion $\log(1 - q_n) = -q_n + o(q_n)$, one finds

$$\log C(n, \lfloor \lambda n \rfloor) \sim \left(\lambda - \frac{3\lambda^3}{\pi^2} \right) n \log n = \frac{\lambda(\pi^2 - 3\lambda^2)}{\pi^2} n \log n.$$

In particular, the leading coefficient changes sign at

$$\lambda_c = \frac{\pi}{\sqrt{3}} \approx 1.81,$$

suggesting that $2n$ -point no-three-in-line configurations should become rare as n grows. Moreover, using the exact expression for t_n , we find that the heuristic count $C(n, 2n)$ becomes smaller than one once $n \geq 493$. While this crude heuristic should not be taken too seriously, we note that $n = 60$ is still far below the suspected threshold where $D(n) = 2n$ might fail.

Maybe more importantly, if one additionally incorporates rotational symmetry into this heuristic (180-degree symmetry suffices), the expected number of solutions drops immediately below one, even though solutions having rotational symmetry clearly exist. This exposes a clear weakness of this heuristic and casts doubts as to its validity.

2. Results and formulations

2.1. Satisfiability formulation

Let $[n]_0 := \{0, 1, \dots, n-1\} \subset \mathbb{Z}$ and $G_n := [n]_0^2 \subset \mathbb{Z}^2$. Associate a binary variable $x_{ij} \in \{0, 1\}$ to each $(i, j) \in G_n$, where $x_{ij} = 1$ indicates that (i, j) is occupied. For $q \geq 2$ define

$$\mathcal{L}_{\geq q}^n := \{\ell \subset \mathbb{R}^2 : \ell \text{ is an affine line and } |\ell \cap G_n| \geq q\}.$$

The no-three-in-line problem can be written as the integer program

$$D(n) := \max \left\{ \sum_{(i,j) \in G_n} x_{ij} : \sum_{(i,j) \in \ell \cap G_n} x_{ij} \leq 2 \quad \forall \ell \in \mathcal{L}_{\geq 3}^n \right\}.$$

Since no-three-in-line implies ≤ 2 per row, any configuration with $2n$ points must have exactly two points in every row. Therefore we also consider the satisfiability variant obtained by enforcing this explicitly:

$$\mathcal{F}_n := \left\{ (x_{ij})_{(i,j) \in G_n} \in \{0, 1\}^{G_n} : \begin{array}{l} \sum_{(i,j) \in \ell \cap G_n} x_{ij} \leq 2 \quad \forall \ell \in \mathcal{L}_{\geq 3}^n, \\ \sum_{i \in [n]_0} x_{ij} = 2 \quad \forall j \in [n]_0 \end{array} \right\}. \quad (1)$$

2.2. Existence up to $n = 60$

Theorem 1. For $2 \leq n \leq 60$ there exists a configuration in \mathcal{F}_n . In particular, $D(n) = 2n$ for $2 \leq n \leq 60$.

Proof. For $n \leq 46$ and for $n \in \{48, 50, 52\}$ the existence of configurations with $D(n) = 2n$ is given in [5, 6]. Table 1 supplies configurations in \mathcal{F}_n for the remaining values $n \in \{47, 49, 51, 53, 54, 55, 56, 57, 58, 59, 60\}$. Since $D(n) \leq 2n$, this implies $D(n) = 2n$ for all $2 \leq n \leq 60$. \square

3. Symmetry reduction

The configurations in Table 1 have additional rotational symmetry. Let $\rho : G_n \rightarrow G_n$ denote the 90° rotation about the center of the grid,

$$\rho(i, j) = (j, n - 1 - i),$$

and let $\langle \rho \rangle$ be the cyclic group it generates. Table 1 lists occupied sites only in a fundamental domain $H_n \subseteq G_n$; the full configuration is obtained by taking the appropriate rotational orbit of each listed site (full $\langle \rho \rangle$ -orbits off-diagonal and $\langle \rho^2 \rangle$ -orbits on the main diagonal when n is odd).

Concretely, define

$$H_n := \begin{cases} [n/2]_0 \times [n/2]_0, & n \text{ even}, \\ [(n+1)/2]_0 \times [(n-1)/2]_0, & n \text{ odd}. \end{cases}$$

Under ρ , a generic site has a $\langle \rho \rangle$ -orbit of size 4. When n is odd we require the anti-diagonal $\{(i, n - 1 - i)\}$ to be empty, and diagonal representatives are expanded only under $\langle \rho^2 \rangle$; these are indicated in boldface in Table 1.

For even n , every site in H_n has a $\langle \rho \rangle$ -orbit of size 4, so choosing $n/2$ orbit representatives in H_n yields $4 \cdot (n/2) = 2n$ occupied sites in G_n . For odd n , off-diagonal sites in H_n have $\langle \rho \rangle$ -orbits of size 4, whereas a diagonal site (i, i) has a $\langle \rho^2 \rangle$ -orbit of size 2. Thus choosing $(n-1)/2$ off-diagonal representatives and one diagonal representative yields $4 \cdot ((n-1)/2) + 2 = 2n$ occupied sites in G_n .

To encode these symmetry requirements in the satisfiability model, introduce binary variables $y_{ij} \in \{0, 1\}$ for $(i, j) \in H_n$ and link them to occupancy variables $x_{kl} \in \{0, 1\}$ on G_n as follows. If n is even, then every $\langle \rho \rangle$ -orbit meets H_n in exactly one site, and we set

$$x_{\rho^t(i,j)} := y_{ij} \quad \text{for all } (i, j) \in H_n \text{ and } t \in \{0, 1, 2, 3\}.$$

If n is odd, we keep the anti-diagonal empty and distinguish off-diagonal and diagonal sites. For $(i, j) \in H_n$ with $i \neq j$ set

$$x_{\rho^t(i,j)} := y_{ij} \quad \text{for } t \in \{0, 1, 2, 3\},$$

while for diagonal sites $(i, i) \in H_n$ set

$$x_{i,i} = x_{\rho^2(i,i)} = x_{n-1-i, n-1-i} := y_{ii},$$

n	
47	$(0, 17), (0, 21), (1, 12), (3, 8), (4, 19), (5, 9), (5, 21), (6, 22), (7, 4), (7, 16), \mathbf{(8, 8)}, (10, 2), (10, 12), (11, 3), (11, 15), (13, 2), (14, 19), (15, 9), (16, 18), (17, 14), (18, 6), (20, 1), (20, 13), (23, 22)$
49	$(0, 13), (1, 18), (2, 9), (3, 5), (4, 2), (5, 20), (6, 16), (6, 18), (10, 4), (10, 7), (11, 15), (11, 19), (12, 9), (13, 14), \mathbf{(15, 15)}, (16, 7), (17, 0), (17, 21), (19, 14), (20, 8), (21, 22), (22, 3), (23, 1), (23, 12), (24, 8)$
51	$\mathbf{(0, 0)}, (0, 20), (2, 13), (4, 14), (4, 23), (5, 9), (6, 5), (7, 18), (10, 9), (10, 12), (11, 8), (13, 22), (14, 6), (15, 1), (15, 22), (16, 2), (16, 8), (17, 12), (18, 23), (19, 3), (20, 17), (21, 3), (21, 11), (24, 1), (24, 7), (25, 19)$
53	$(0, 16), (0, 20), (2, 20), (2, 25), (3, 24), \mathbf{(5, 5)}, (5, 8), (6, 14), (6, 24), (7, 8), (7, 21), (9, 10), (11, 3), (13, 9), (13, 19), (14, 17), (15, 1), (15, 22), (17, 12), (18, 1), (18, 12), (19, 4), (21, 4), (22, 11), (23, 10), (23, 25), (26, 16)$
54	$(0, 22), (0, 24), (2, 16), (3, 7), (3, 24), (4, 15), (5, 11), (6, 17), (8, 25), (9, 5), (9, 6), (11, 14), (12, 2), (12, 13), (13, 21), (17, 4), (18, 10), (18, 16), (19, 1), (19, 10), (20, 8), (20, 15), (22, 1), (23, 7), (23, 14), (25, 26), (26, 21)$
55	$(2, 14), (3, 18), \mathbf{(4, 4)}, (4, 18), (5, 9), (6, 2), (6, 11), (7, 26), (8, 19), (8, 20), (9, 25), (10, 13), (11, 13), (12, 3), (12, 21), (14, 16), (15, 10), (17, 20), (17, 24), (19, 1), (22, 5), (22, 7), (23, 1), (23, 15), (24, 16), (25, 0), (26, 0), (27, 21)$
56	$(1, 5), (2, 13), (3, 1), (3, 27), (5, 26), (6, 17), (7, 23), (8, 20), (9, 10), (9, 14), (10, 19), (12, 0), (12, 21), (14, 11), (16, 6), (16, 21), (17, 24), (18, 4), (18, 11), (19, 15), (20, 7), (22, 2), (22, 4), (23, 24), (25, 8), (25, 15), (26, 13), (27, 0)$
57	$(1, 23), (3, 24), (4, 6), (4, 24), (5, 16), (5, 18), (6, 3), (7, 11), (8, 16), (8, 26), (9, 2), \mathbf{(10, 10)}, (12, 0), (12, 21), (13, 7), (13, 17), (14, 15), (14, 26), (15, 17), (19, 10), (19, 11), (20, 1), (20, 25), (22, 21), (23, 2), (25, 0), (27, 9), (27, 22), (28, 18)$
58	$(1, 14), (1, 19), (2, 19), (3, 26), (3, 27), (5, 15), (6, 5), (7, 18), (8, 4), (10, 7), (11, 4), (12, 15), (13, 11), (13, 18), (14, 22), (16, 21), (17, 2), (17, 8), (20, 6), (20, 24), (21, 0), (22, 16), (23, 23), (25, 9), (25, 10), (26, 24), (27, 0), (28, 9), (28, 12)$
59	$(0, 12), (1, 26), (2, 27), (3, 15), (4, 7), (5, 21), (5, 25), (7, 14), (8, 16), (8, 26), \mathbf{(9, 9)}, (9, 11), (10, 4), (10, 27), (12, 16), (13, 6), (14, 18), (15, 25), (18, 17), (19, 6), (20, 1), (21, 11), (22, 17), (23, 3), (23, 20), (24, 0), (24, 13), (28, 19), (28, 22), (29, 2)$
60	$(0, 20), (3, 15), (3, 19), (4, 26), (5, 9), (6, 8), (6, 23), (7, 29), (8, 18), (10, 5), (11, 21), (12, 12), (13, 0), (13, 7), (15, 27), (16, 23), (16, 25), (17, 2), (17, 11), (18, 4), (19, 14), (20, 1), (21, 24), (22, 9), (24, 1), (25, 27), (26, 22), (28, 2), (28, 10), (29, 14)$

Table 1: Representatives of occupied-site orbits. Here $\rho(i, j) = (j, n - 1 - i)$ is the 90° rotation about the center $(\frac{n-1}{2}, \frac{n-1}{2})$. For n odd, bold entries lie on the main diagonal and generate 2-cycles under ρ^2 ; the anti-diagonal is empty. The full configuration is obtained by applying ρ (off-diagonal entries) or ρ^2 (bold diagonal entries for odd n) to each representative.

and enforce

$$x_{i, n-1-i} = 0 \quad \text{for all } i \in [n]_0.$$

Equivalently, for $(i, j) \in H_n$ define

$$O(i, j) := \begin{cases} \{\rho^t(i, j) : t = 0, 1, 2, 3\}, & \text{if } n \text{ is even or } i \neq j, \\ \{(i, i), \rho^2(i, i)\} = \{(i, i), (n-1-i, n-1-i)\}, & \text{if } n \text{ is odd and } i = j, \end{cases}$$

and for odd n let $A_n := \{(i, n-1-i) : i \in [n]_0\}$ denote the anti-diagonal. Then all sites in $O(i, j)$ share the common value y_{ij} , and all sites in A_n are fixed to 0.

Let $\Gamma_n := \langle \rho \rangle$ if n is even and $\Gamma_n := \langle \rho^2 \rangle$ if n is odd. Let $\mathcal{L}_{\geq 3}^{n, \Gamma} \subseteq \mathcal{L}_{\geq 3}^n$ be a choice of one representative from each Γ_n -orbit of lines in $\mathcal{L}_{\geq 3}^n$.

For any affine line $\ell \subset \mathbb{R}^2$ define

$$c_\ell(i, j) := |\ell \cap O(i, j)| \quad ((i, j) \in H_n),$$

and for any row index $r \in [n]_0$ define

$$d_r(i, j) := |\{(k, r) \in O(i, j)\}| \quad ((i, j) \in H_n).$$

The reduced satisfiability model becomes

$$\mathcal{F}_n^{\text{sym}} := \left\{ (y_{ij})_{(i,j) \in H_n} \in \{0, 1\}^{H_n} : \begin{array}{l} \sum_{(i,j) \in H_n} c_\ell(i, j) y_{ij} \leq 2 \quad \forall \ell \in \mathcal{L}_{\geq 3}^{n, \Gamma}, \\ \sum_{(i,j) \in H_n} d_r(i, j) y_{ij} = 2 \quad \forall r \in [n]_0 \end{array} \right\}. \quad (2)$$

4. Implementation and computational setup

Although the no-three-in-line problem is classical, obtaining new exact results via a general-purpose CP-SAT solver is not a black-box exercise. The formulation given earlier is necessary but, in practice, far from sufficient: whether an instance is solved quickly or not at all can hinge on details of solver behaviour that are largely invisible at the level of the mathematical model, such as the interaction between propagation, cutting, branching, restarts, and the solver's internal portfolio of search strategies. These mechanisms are not designed with this particular combinatorial geometry problem in mind, and their effective use therefore requires problem-specific experimentation and an understanding of what aspects of the instance structure the solver is able (or unable) to exploit.

For this reason we describe our implementation choices and computational protocol in some detail. Beyond enabling verification and reproducibility, these details are intended to be methodological: many combinatorial problems admit compact constraint formulations yet remain computationally intractable unless one knows how to present the structure to a modern solver and how to interpret its stochastic and heavy-tailed runtime behaviour. We expect that the modelling decisions, symmetry handling, and restart/parallelisation strategy discussed below will be relevant to researchers aiming to apply CP-SAT-type technology to other exact search problems in combinatorics, where the same “model correctness versus solver effectiveness” gap frequently determines what can be proved computationally.

4.1. Hardware and software

Most computations reported here were carried out on an AMD EPYC 9965 CPU (192 cores, 384 threads) with 2.2 TB RAM. Unless stated otherwise, run times refer to this architecture and are measured as wall-clock time to first solution when running 384 independent solver instances in parallel. All CP-SAT runs use a single search worker per instance (i.e. no internal parallelism within a CP-SAT run). In cases when runs were terminated after the maximal job length of ten days, or when runs were distributed over cores of several other HPC machines, a heuristic composite runtime equivalent was used.

4.2. Constraint generation and deduplication

Implementing the satisfiability model (1) is straightforward, and a closely related mixed integer programming formulation was previously solved with Gurobi [4]. The CP-SAT implementation is similar: introduce binary variables x_{ij} and add the linear constraints $\sum_{(i,j) \in \ell \cap G_n} x_{ij} \leq 2$ for each $\ell \in \mathcal{L}_{\geq 3}^n$. The resulting model has n^2 binary variables and $|\mathcal{L}_{\geq 3}^n|$ line constraints. Moreover $|\mathcal{L}_{\geq 3}^n| = \Theta(n^4)$; more precisely, $|\mathcal{L}_{\geq 3}^n| \sim \frac{5}{12\pi^2} n^4$ as $n \rightarrow \infty$ [11]. For comparison, $\binom{n^2}{2}$ is a crude upper bound on the number of distinct lines determined by unordered pairs of grid points, so $|\mathcal{L}_{\geq 3}^n|/\binom{n^2}{2} \rightarrow 5/(6\pi^2) \approx 0.084$.

In the implementation, each line constraint is represented by its finite intersection set $\ell \cap G_n$. Concretely, we build a dictionary whose keys are canonical encodings of distinct intersection sets $\ell \cap G_n$, and whose values store the corresponding lists of lattice points. The resulting collection of constraints is then passed to CP-SAT as linear inequalities. The computational cost of generating these constraints and performing this deduplication is negligible compared with the subsequent solver runtime for the instances considered here.

After rewriting constraints in terms of orbit variables y_{ij} in the symmetry-reduced model (2), further accidental coincidences can occur: distinct representatives $\ell \in \mathcal{L}_{\geq 3}^{n,\Gamma}$ may induce the same incidence vector $(c_\ell(i,j))_{(i,j) \in H_n}$ on H_n and hence the same linear inequality. We therefore optionally deduplicate again at this stage by keeping one representative per distinct incidence vector (CP-SAT tolerates the redundancy either way). In addition, some line inequalities become tautological after symmetry reduction (for example, if enforcing an empty anti-diagonal reduces $\ell \cap G_n$ to at most two unfixed orbit sites), and these can be discarded outright since $\sum_{(i,j) \in H_n} c_\ell(i,j) y_{ij} \leq 2$ then holds automatically for $y_{ij} \in \{0, 1\}$.

4.3. Model sizes

Table 2 illustrates the substantial reduction in model size obtained by enforcing rotational symmetry. The number of variables drops from n^2 to $|H_n|$, i.e. by a factor close to four (exactly 4 for even n , and $(n^2 - 1)/4$ for odd n). The number of constraints is reduced by roughly the same factor, reflecting both the smaller variable set and the restriction to a representative family of line constraints (with further deduplication after rewriting in orbit variables).

n	Binary variables		Constraints	
	no restriction	symmetry	no restriction	symmetry
2	4	1	2	2
3	9	2	8	3
4	16	4	14	6
5	25	6	32	12
\vdots	\vdots	\vdots	\vdots	\vdots
56	3136	784	415230	103868
57	3249	812	446296	118241
58	3364	841	476358	119160
59	3481	870	510756	135183
60	3600	900	546354	136660

Table 2: Model sizes for the satisfiability formulation (1) (“no restriction”) and its rotationally symmetric reduction (2) (“symmetry”). The table reports the number of Boolean decision variables and the number of linear constraints in each model. Constraint counts include the n row equalities enforcing two occupied sites per row; horizontal line inequalities are not counted separately since they are subsumed by these equalities. In the symmetry-reduced model we additionally discard line inequalities that become tautological after rewriting in orbit variables (e.g. when fewer than three unfixed orbit sites remain on a line).

4.4. Parallel protocol and termination

Our parallel protocol is “run-until-first-success”. Specifically, we launch $M = 384$ independent CP-SAT runs, each with a fresh random seed and a single internal search worker. Runs proceed independently until the first solver reports a feasible solution; at that point the experiment terminates and all remaining solver instances are stopped. Reported wall times therefore correspond to $T_M = \min\{T^{(1)}, \dots, T^{(M)}\}$, measured from a common launch time to the first success.

5. Solve times and scaling

5.1. Baseline timings

As can be seen from Figure 2, without symmetry restrictions the solver finds configurations up to about $n = 20$ within roughly one hour of wall-clock time in this experiment. Restricting the search space to configurations with 90° rotational symmetry (modified as described above for odd n) reduces the model size substantially while still leaving solutions within the reduced model. Together, these reductions make much larger instances tractable: as Figure 2 shows, configurations for $n = 50$ can be found within about one hour.

Since large runs are inherently stochastic, we now quantify the distribution of solve times for the symmetry-reduced model (2) and use it for a tentative extrapolation to larger n .

5.2. Empirical solve-time distributions and parallelism

Let T denote the wall-clock time to the first solution in a single CP-SAT run (with a fresh random seed), and write $F(t) = \mathbb{P}(T \leq t)$ for its cumulative distribution function

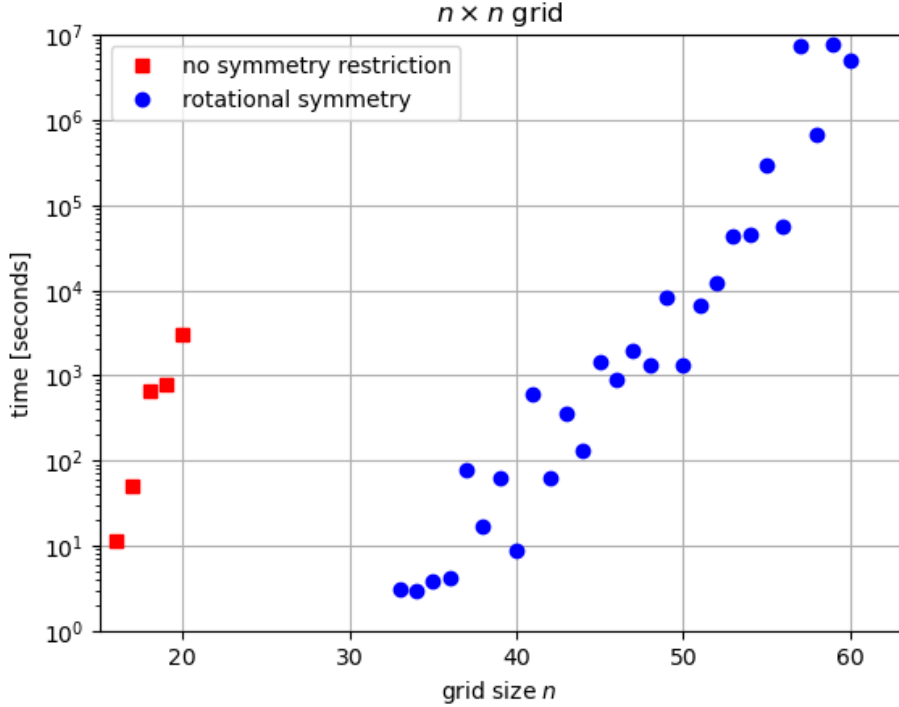


Figure 2: Wall-clock time (log scale) to the first solution in a single experiment consisting of 384 independent CP-SAT runs executed in parallel on an AMD EPYC 9965 CPU. Red squares: direct model (1) (no symmetry restriction). Blue circles: symmetry-reduced model (2) enforcing rotational symmetry.

and $S(t) = 1 - F(t)$ for the survival function. When running M independent solver instances in parallel, the time to the first solution is

$$T_M := \min\{T^{(1)}, \dots, T^{(M)}\},$$

and therefore

$$S_M(t) = \mathbb{P}(T_M > t) = S(t)^M, \quad \text{equivalently} \quad F_M(t) = 1 - (1 - F(t))^M. \quad (3)$$

Thus, the small- t behaviour of $F(t)$ controls the practically relevant distribution $F_M(t)$.

Data collection protocol. For $n = 33, \dots, 44$ we generated empirical solve-time distributions by first running a brief pilot to identify a cutoff time τ such that $F_{384}(\tau)$ was roughly 0.99. We then ran a larger batch of independent single-run experiments with this single cutoff. Over the time windows shown in Figures 3 and 4, censoring effects are negligible on the scales relevant for $F_{384}(t)$, and we compute $F(t)$ directly from the observed completion times. (If heavy censoring were present—for example, if a substantial fraction of runs timed out before completion—then a Kaplan–Meier estimator would be the appropriate replacement; we did not need this here.)

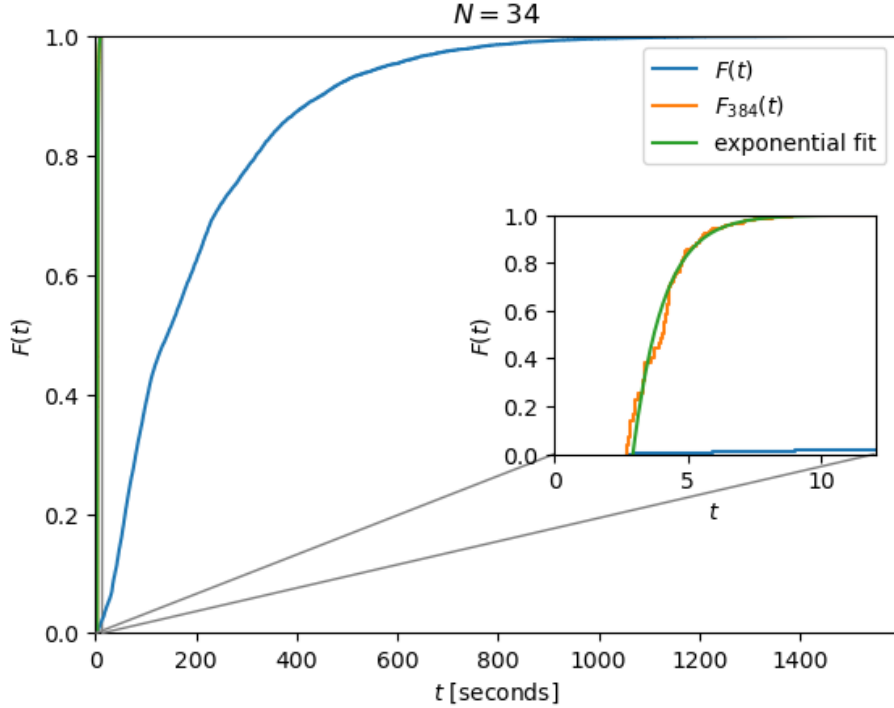


Figure 3: Empirical cumulative distribution function $F(t)$ of the time to success for a single CP-SAT run (blue), obtained from 10,436 independent runs of (2) at $n = 34$. Also shown is the derived CDF $F_{384}(t)$ for the first success among $M = 384$ parallel runs (orange), computed via (3), and a shifted-exponential fit (4) to $F_{384}(t)$ near the origin (green). The inset magnifies the small-time region relevant for F_{384} .

Figure 3 illustrates this transformation for $n = 34$. The blue curve is the empirical single-run CDF $F(t)$, while the orange curve is the derived $F_{384}(t)$ computed from (3). The latter concentrates heavily at small times: a small success probability per run is amplified into a large success probability for the parallel experiment.

5.3. A shifted-exponential model

Motivated by the near-linearity of $-\log(1 - F_{384}(t))$ over the early-time regime, we model T_M by a shifted exponential distribution,

$$F_M^{\text{exp}}(t) = \begin{cases} 0, & t \leq t_0, \\ 1 - \exp\left(-\frac{M(t - t_0)}{t_1}\right), & t > t_0, \end{cases} \quad (4)$$

where t_0 captures an effective deterministic overhead (model construction, presolve, initial propagation, etc.) and t_1 is a characteristic “delay” scale. If the underlying single-run time T itself were shifted exponential with the same t_0 and t_1 , then (4) would follow exactly from (3); here we use (4) primarily as an accurate description of the empirical $F_M(t)$ for small t .

For T_M distributed as (4), the mean and quantiles are explicit. In particular,

$$\mathbb{E}[T_M] = t_0 + \frac{t_1}{M}, \quad t_p := F_M^{-1}(p) = t_0 + \frac{t_1}{M} \log\left(\frac{1}{1-p}\right). \quad (5)$$

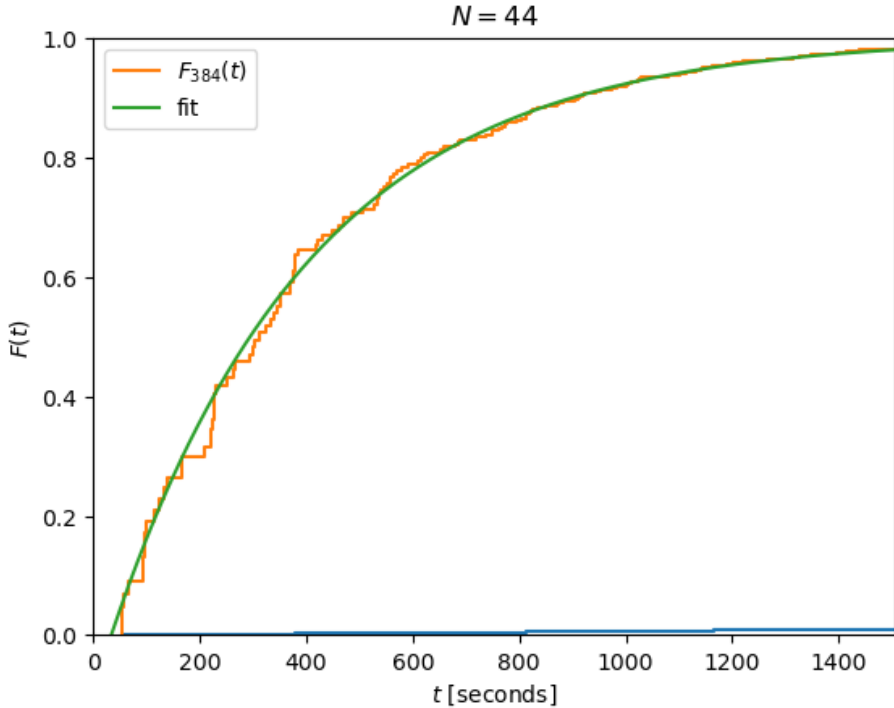


Figure 4: For $n = 44$: derived CDF $F_{384}(t)$ for the first success among 384 parallel runs (orange) together with a shifted-exponential fit (4) (green). On this time window the empirical single-run CDF $F(t)$ is extremely small and is therefore not visually prominent.

5.4. Parameter growth and extrapolation

Table 3 reports the fitted parameters (t_0, t_1) for even n from 34 to 44, together with the implied mean time to first solution for $M = 384$ parallel runs, $\mathbb{E}[T_{384}]$ from (5). While the fitted threshold t_0 grows moderately, the delay scale t_1 grows rapidly; for $n = 44$ it already exceeds 40 hours, even though $\mathbb{E}[T_{384}]$ remains on the order of minutes.

For practical scheduling, quantiles are more relevant than the mean. Using (5), the median and 98% quantile of T_M are

$$t_{0.5} = t_0 + \frac{t_1}{M} \log 2, \quad t_{0.98} = t_0 + \frac{t_1}{M} \log 50.$$

Figure 5 plots, on a semi-logarithmic scale, (i) observed single-run solve times for the instances considered, and (ii) the estimated 50% and 98% completion times for $M = 384$ parallel runs. Least-squares fits of $\log t$ against n over the measured range suggest

n	t_0 [s]	t_1 [s]	$t_0 + t_1/384$ [s]
34	2.92	550.61	4.36
36	3.70	1721.67	8.18
38	6.77	6029.78	22.47
40	10.96	12016.51	42.25
42	29.79	24653.03	93.99
44	33.24	144613.52	409.84

Table 3: Fitted threshold time t_0 and delay time scale t_1 for even $n = 34, 36, \dots, 44$, using the shifted-exponential model (4). The final column is the implied mean time to first solution when running $M = 384$ solvers in parallel, cf. (5).

an approximately exponential growth of these quantiles with n . Extrapolating these fits gives a rough indication of which sizes may be reachable within a fixed wall-clock budget (here indicated by a ten-day line). We emphasize that this extrapolation is heuristic: modest curvature in the semi-log plot would translate into large changes at the extrapolated sizes.

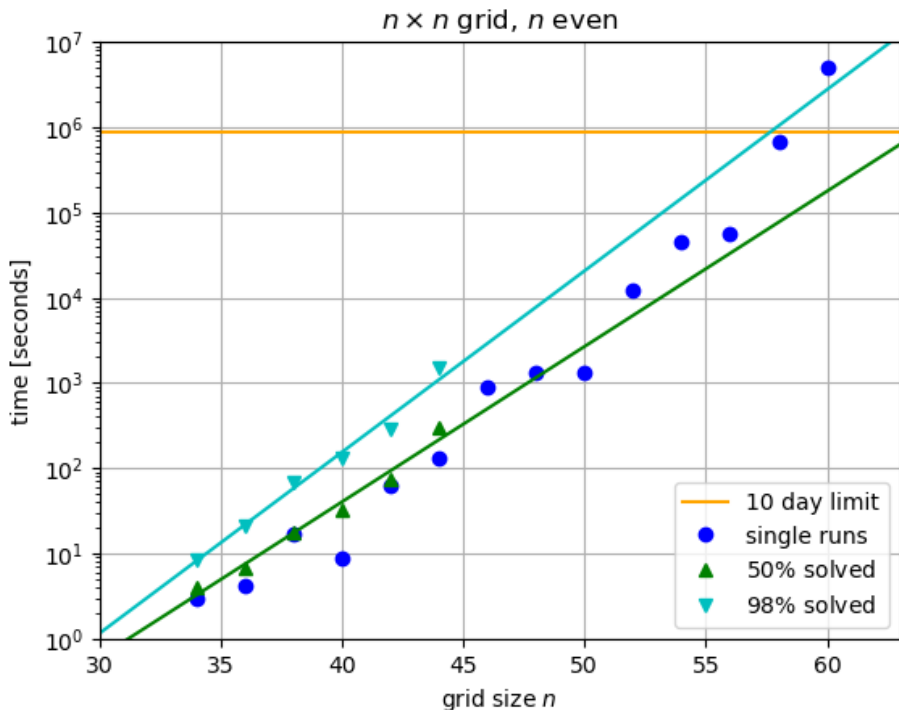


Figure 5: Even sizes: semi-log plot of solve-time statistics versus grid size n . Blue circles: observed wall-clock times to first solution in single runs. Green triangles and cyan inverted triangles: estimated 50% and 98% completion times for $M = 384$ parallel runs, derived from the shifted-exponential fit (4) via (5). Solid lines: least-squares fits of $\log t$ versus n . The horizontal line indicates a ten-day wall-clock budget. Reported times over 10 days are aggregated from multiple job runs.

Even and odd n behave differently under our enforced symmetry (for odd n only $\Gamma_n = \langle \rho^2 \rangle$ is imposed on diagonal variables), so we analyse odd sizes separately. Figure 6 presents the analogous semi-log plot for odd n (with fits obtained over the measured range). The extrapolations are consistent with our computational results: odd sizes up to $n = 59$ are found within the ten-day horizon under the same parallel regime.

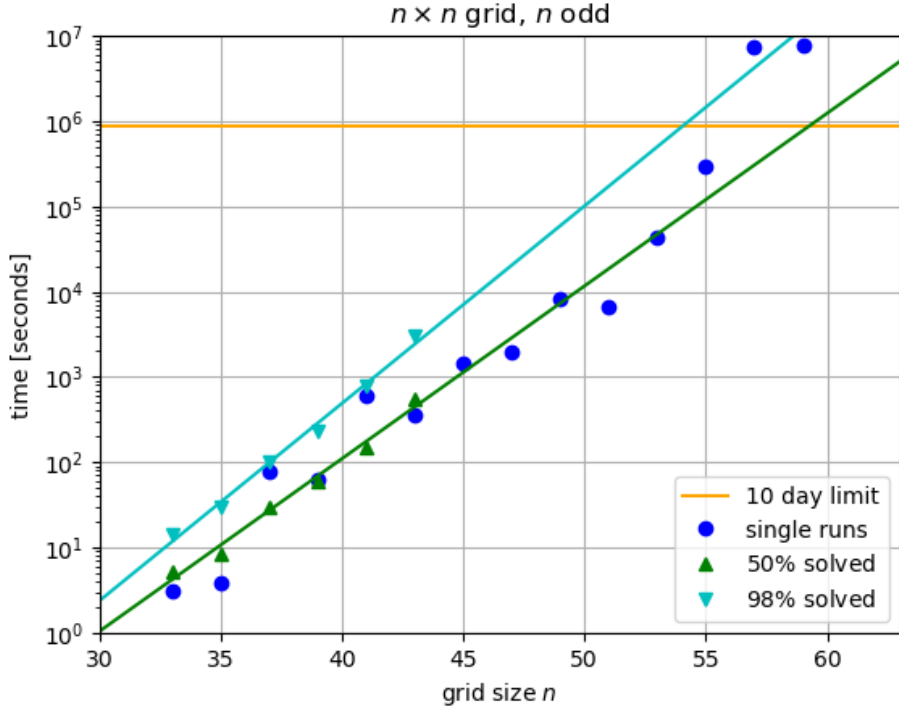


Figure 6: Odd sizes: solve-time statistics versus grid size n , shown as in Figure 5. Because the enforced symmetry is weaker for odd n , the corresponding solve-time growth differs, motivating separate fits.

5.5. Attempts at further speedups

Given the effectiveness of CP-SAT on this problem, we explored several refinements. CP-SAT exposes a large number of parameters, but in our experiments parameter changes did not produce improvements beyond statistical variation. In line with standard practice, we also ran portfolios of parameter choices (a “hedging” strategy) for large n , again without a consistent speedup.

We additionally tested: (i) mild guidance via objective functions or branching priorities derived from empirical density profiles; (ii) for even n , constraints fixing the number of occupied sites on the diagonals; (iii) “anchoring” selected sites; and (iv) warm starts based on partial configurations. None of these improved performance reliably, and some were detrimental. In particular, warm-starting an instance at size $n + 2$ by embedding a solution at size n often caused the search to stall.

Overall, the best-performing strategy was to allow the solver to operate with minimal external interference. While CP-SAT is partly a black box, its strength is widely attributed to the dynamic generation of cutting planes and learned clauses during search. External restrictions can change the search trajectory and may inhibit this mechanism, offering a plausible explanation for the negative results of several “helper” constraints in our setting.

6. Conclusion and outlook

We have shown, using a symmetry-reduced CP-SAT formulation, that configurations with $2n$ points and no three collinear exist on the $n \times n$ grid for all $n \leq 60$. Combined with earlier results for $n \leq 46$ and $n \in \{48, 50, 52\}$, this raises the smallest n for which it is currently unknown whether $D(n) = 2n$ from 47 to 61.

From a computational perspective, enforcing rotational symmetry reduces the satisfiability model by roughly a factor of four in both variables and constraints and makes sizes near $n = 60$ tractable on modern many-core hardware. Empirically, for parallel “run-until-first-success” experiments, the early-time behaviour of the solve-time distribution is well described by a shifted-exponential model, allowing quantiles relevant for scheduling to be estimated and (heuristically) extrapolated. The resulting extrapolations are suggestive but should be interpreted cautiously: mild curvature in the semi-log scaling plots would substantially change predictions at larger sizes.

The remaining open problem is to determine whether $D(61) = 122$ (and beyond). We attempted $n = 61$ and $n = 62$ with the current method; however, no solution was found within 10^7 seconds, so we are leaving this as an open case.

On the algorithmic side, an interesting direction is to identify additional structure (beyond rotational symmetry) that reduces the search space without eliminating solutions, or to design hybrid approaches that exploit learned constraints while preserving the solver’s ability to generate effective clauses during search.

Data and software availability

The configurations listed in Table 1 are representatives of rotational orbits and can be expanded to full configurations as described in Section 3.

A reference implementation of the CP-SAT model described in this manuscript was generated from the mathematical specification and implementation details in the text using an LLM-based coding assistant (ChatGPT). The generated code was then run and validated against a verification program and against the reported configurations and timings. This code and the configuration data from Table 1 are available at

- <https://github.com/ThomasPrellberg/no-three-in-line---CP-SAT>

to facilitate reproducibility. Independent verification of each listed configuration takes seconds and does not rely on CP-SAT.

Declaration of competing interest

The author declares no competing interests.

Acknowledgements

This research utilized Queen Mary's Apocrita HPC facility, supported by QMUL Research-IT, <http://doi.org/10.5281/zenodo.438045>.

Declaration of generative AI and AI-assisted technologies in the manuscript preparation process

During the preparation of this work the author used OpenAI ChatGPT (ChatGPT Plus) in order to generate Python code implementing (1) and (2), and to assist with editorial checks and content organization. After using this tool/service, the author reviewed and edited the content as needed and takes full responsibility for the content of the published article.

References

- [1] U. Chandran S.V., S. Klavžar, J. Tuite, The General Position Problem: A Survey, arXiv:2501.19385 (2025).
- [2] F. Charton, J.S. Ellenberg, A.Z. Wagner, G. Williamson, PatternBoost: Constructions in Mathematics with a Little Help from AI, arXiv:2411.00566 (2024).
- [3] H. Dudeney, Amusements in Mathematics, Nelson, Edinburgh, 1917.
- [4] D. Eppstein, Gurobi versus the no-three-in-line problem, blog post, November 12, 2018, <https://11011110.github.io/blog/2018/11/12/gurobi-vs-no.html>.
- [5] A. Flammenkamp, Progress in the no-three-in-line problem, *J. Combin. Theory Ser. A* 60 (1992) 305–311.
- [6] A. Flammenkamp, Progress in the No-Three-in-Line Problem, II, *J. Combin. Theory Ser. A* 81 (1998) 108–113.
- [7] R.K. Guy, P.A. Kelly, The no-three-in-line problem, *Canadian Math. Bull.* 11 (1968) 527–531.
- [8] R.K. Guy, Unsolved Problems in Number Theory, Springer-Verlag, New York, Heidelberg, Berlin, 1981.
- [9] R.R. Hall, T.H. Jackson, A. Sudbery, K. Wild, Some advances in the no-three-in-line problem, *J. Combin. Theory Ser. A* 18 (1975) 336–341.
- [10] H. Harborth, P. Oertel, T. Prellberg, No-three-in-line for seventeen and nineteen, *Discrete Math.* 73 (1988/89) 89–90.
- [11] P. Haukkanen, J.K. Merikoski, Asymptotics for numbers of line segments and lines in a square grid, *Int. J. Number Theory* 8 (2012) 1145–1152.
- [12] Y.C.R. Lin, On the general no-three-in-line problem, arXiv:2106.15621 (2021).

- [13] W. Moser, J. Pach, Research Problems in Discrete Geometry, McGill University, Montreal, 1986.
- [14] D.T. Nagy, Z.L. Nagy, R. Woodroffe, The extensible No-Three-In-Line problem, European J. Combin. 111 (2023) 103796.
- [15] L. Perron, F. Didier, CP-SAT (version 9.12), Google, 2025. https://developers.google.com/optimization/cp/cp_solver/.
- [16] P. Ramanathan, T. Prellberg, M. Lewis, C. Beck, P.D. Joshi, R.A. Dandekar, R. Dandekar, S. Panat, Three methods, one problem: Classical and AI approaches to no-three-in-line, arXiv:2512.11469 (2025).